Glucose transporter inhibitor-conjugated insulin mitigates hypoglycemia

Jinqiang Wang[a,b], Jicheng Yu[c], Yuqi Zhang[c], Anna R. Kahkoska[d], Zejun Wang[a,b], Jun Fang[a], Julian P. Whitelegge[e], Song Li[a,f], John B. Buse[d], and Zhen Gu[a,b,g,h,1]

[a]Department of Bioengineering, University of California, Los Angeles, CA 90095; [b]California NanoSystems Institute, University of California, Los Angeles, CA 90095; [c]Joint Department of Biomedical Engineering, University of North Carolina at Chapel Hill and North Carolina State University, Raleigh, NC 27514; [d]Department of Medicine, University of North Carolina School of Medicine, Chapel Hill, NC 27599; [e]The Pasarow Mass Spectrometry Laboratory, The Jane and Terry Semel Institute for Neuroscience and Human Behavior, David Geffen School of Medicine, University of California, Los Angeles, CA 90095; [f]Department of Medicine, University of California, Los Angeles, CA 90095; [g]Jonsson Comprehensive Cancer Center, University of California, Los Angeles, CA 90024; and [h]Center for Minimally Invasive Therapeutics, University of California, Los Angeles, CA 90095

Edited by Hongjie Dai, Department of Chemistry, Stanford University, Stanford, CA, and approved April 17, 2019 (received for review February 4, 2019)

Insulin therapy in the setting of type 1 and advanced type 2 diabetes is complicated by increased risk of hypoglycemia. This potentially fatal complication could be mitigated by a glucose-responsive insulin analog. We report an insulin-facilitated glucose transporter (Glut) inhibitor conjugate, in which the insulin molecule is rendered glucose-responsive via conjugation to an inhibitor of Glut. The binding affinity of this insulin analog to endogenous Glut is modulated by plasma and tissue glucose levels. In hyperglycemic conditions (e.g., uncontrolled diabetes or the postprandial state), the in situ-generated insulin analog–Glut complex is driven to dissociate, freeing the insulin analog and glucose-accessible Glut to restore normoglycemia. Upon overdose, enhanced binding of insulin analog to Glut suppresses the glucose transport activity of Glut to attenuate further uptake of glucose. We demonstrate the ability of this insulin conjugate to regulate blood glucose levels within a normal range while mitigating the risk of hypoglycemia in a type 1 diabetic mouse model.

drug delivery | diabetes | glucose-responsive | insulin | insulin analog

Diabetes mellitus affects more than 400 million people across the world (1–3). The treatment for type 1 and advanced type 2 diabetes is multiple daily injections or continuous infusion of exogenous insulin (1, 2, 4). However, the benefits of insulin therapy are often not fully realized, due to the risk of hypoglycemia associated with insulin overdose, which can result in seizure, coma, and death (5). Therefore, tremendous efforts have been devoted to the development of smart insulin delivery systems that mimic the glucose-dependent dynamic insulin secretion of β-cells, thereby reducing hyperglycemic condition and mitigating the risk of insulin-induced hypoglycemia associated with a miscalculated exogenous insulin dose (6, 7). To this end, chemically driven synthetic closed-loop insulin delivery systems integrating phenylboronic acid (7–16), glucose-binding protein (17–20), and glucose oxidase (21–26) have been extensively studied. However, synthetic strategies to tightly regulate blood glucose levels with a low risk of hypoglycemia remain elusive in clinical practice (27).

Here, we propose to expand the safety margin of insulin by simply conjugating insulin with a reversible glucose transporter (Glut) inhibitor. Glut is a family of transmembrane proteins that facilitate the transport of glucose across plasma membranes (28). Various compounds are able to competitively inhibit the glucose transport activity of Glut (29–31). Due to the presence of the Glut inhibitor, the insulin analog can reversibly and dynamically bind to Glut on cell membranes with an affinity modulated by surrounding glucose concentration, rendering the insulin molecule glucose-responsive (Fig. 1). Upon s.c. injection, this insulin analog can bind to insulin receptors (IR) as well as endogenous Glut, establishing an in situ-generated reservoir of insulin analog–Glut complex (Fig. 1). Upon a glucose challenge, such as the glucose rise associated with a meal, the insulin analog–Glut complexes dissociate to liberate free Glut on plasma membranes as well as free insulin analog into interstitial fluids and plasma. The free insulin analog can subsequently bind to IR to trigger the translocation of Glut4 to cell membranes and enhance glucose clearance into muscle and fat. Meanwhile, the Glut, which is previously inaccessible to glucose as part of the insulin analog–Glut complex, can enhance the blood glucose clearance. In excess doses, the insulin analog induces overexpression of Glut on plasma membranes and subsequently triggers the glucose uptake by cells, which could potentially induce hypoglycemia; however, the formation of the glucose-responsive insulin analog–Glut complexes can suppress the glucose transport efficiency of Glut, therefore reducing the hypoglycemic risk.

Results

Glut-i2, a reversible Glut inhibitor with a low dissociation constant and high affinity for Glut4 and Glut1 (32), was selected for our study. Glut-i2 was integrated with a single terminal amino group to give Glut-i2–NH_2 (*SI Appendix*, Scheme S1 and Figs. S1–S5) (32). Next, Glut-i2–NH_2 was conjugated to insulin via a bifunctional linker (17) succinimidyl 4-(*N*-maleimidomethyl)cyclohexane-1-carboxylate to give insulin–Glut-i2 conjugate (designated *i*-insulin), which was confirmed by measuring the molecular weight via the matrix-assisted laser desorption/ionization with a time-of-flight analyzer (*SI Appendix*, Fig. S6), while the modification was validated on A1 of insulin (*SI Appendix*, Fig. S7).

To test the binding ability of the *i*-insulin toward Glut, it was labeled with sulfo-Cyanine 5 (Cy5-*i*-insulin) and used to treat erythrocyte ghost, a widely used Glut carrier (*SI Appendix*, Fig. S8) (33, 34). After 30-min incubation with *i*-insulin at room temperature, the erythrocyte ghosts showed a high fluorescence

Significance

Glucose-responsive insulin analogs or delivery systems are desirable for enhancing health and improving quality of life of people with diabetes. We describe here a simple strategy to engineer a long-acting insulin analog, which can establish an endogenous Glut-associated delivery reservoir of insulin that can modulate glucose metabolism in a blood glucose-dependent manner. Importantly, after subcutaneous injection, in vivo blood glucose regulation was validated in a type 1 diabetic mouse model with negligible hypoglycemia.

Author contributions: J.W., J.Y., and Z.G. designed research; J.W., J.Y., Z.W., J.F., and J.P.W. performed research; J.W., J.Y., Y.Z., A.R.K., S.L., J.B.B., and Z.G. analyzed data; and J.W., J.Y., Y.Z., A.R.K., S.L., J.B.B., and Z.G. wrote the paper.

Conflict of interest statement: J.W. and Z.G. have applied for patents related to this study.

This article is a PNAS Direct Submission.

Published under the PNAS license.

[1]To whom correspondence should be addressed. Email: guzhen@ucla.edu.

This article contains supporting information online at www.pnas.org/lookup/suppl/doi:10.1073/pnas.1901967116/-/DCSupplemental.

Published online May 16, 2019.

PNAS PNAS PNAS PNAS

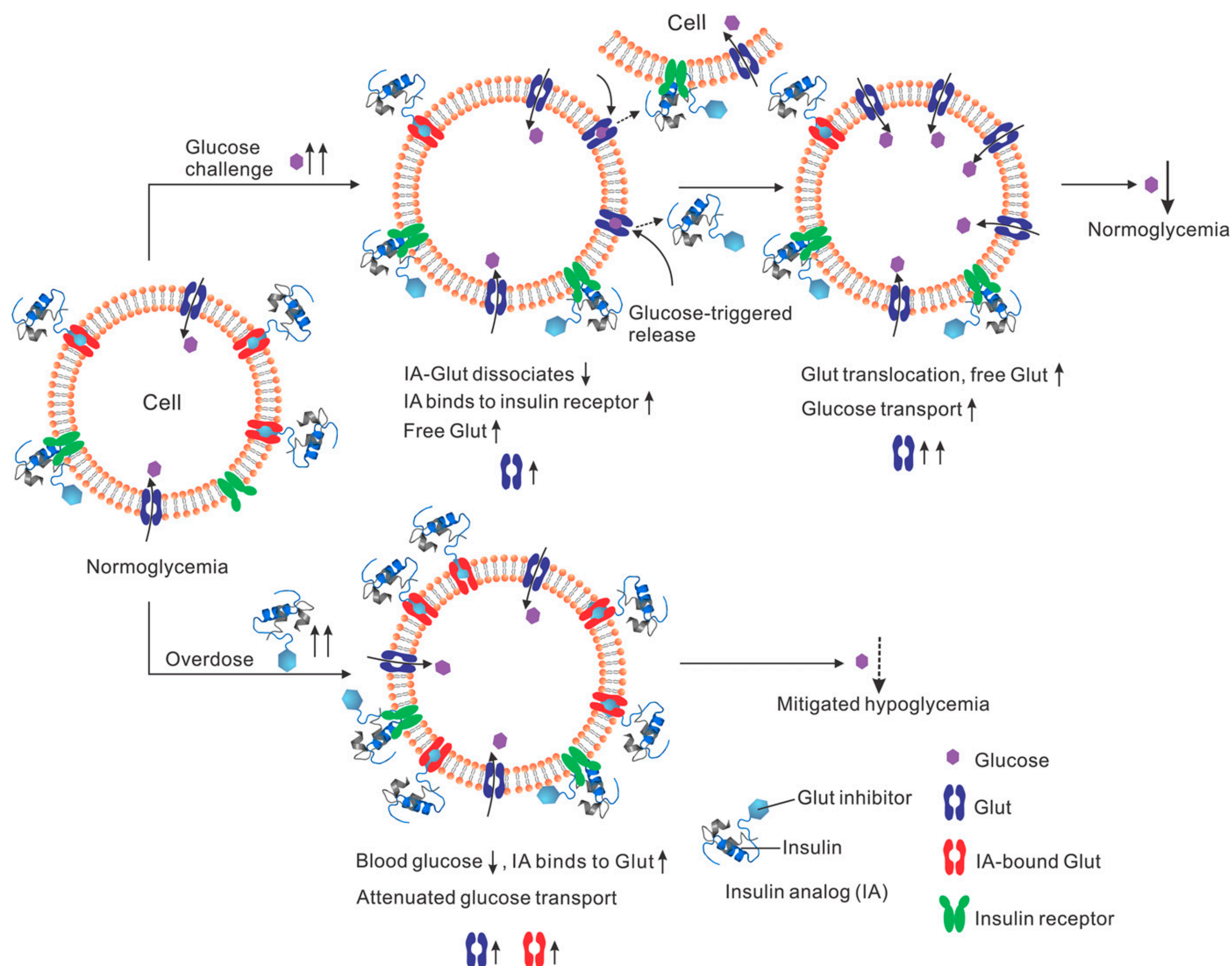

Fig. 1. Schematic of regulating the glucose-transport activity with insulin analog (IA; in this study, *i*-insulin serves as a model analog). Insulin analog can bind to Glut in a glucose-responsive manner. Upon injection and in normoglycemia, insulin analog achieves a regular blood glucose clearance rate, and an insulin analog–Glut complex reservoir is formed. Upon a glucose challenge, increased blood glucose levels result in the release of insulin analog from the insulin analog–Glut complex, which subsequently binds to IR to trigger the translocation of Gluts to cell membranes. With dissociation of insulin analog, glucose-inaccessible insulin analog-bound Glut becomes free Glut, enhancing excess blood glucose clearance. Upon an excess insulin analog injection (i.e., overdose), the formation of the insulin analog–Glut complex attenuates the glucose transport activity of Glut, therefore mitigating hypoglycemia risk.

intensity localized on the membranes, whereas the surrounding solvent showed a slightly weaker fluorescence (Fig. 2*A*). Control erythrocyte ghosts treated with Cy5-labeled native insulin only showed weak fluorescence comparable to the background (Fig. 2*B*). Moreover, the amount of Cy5-*i*-insulin bound to erythrocyte ghosts increased along with the increase of the concentration of free Cy5-*i*-insulin (*SI Appendix*, Fig. S9), and the K_d was measured as 13 nM (*SI Appendix*, Figs. S10 and S11 and Eqs. **S1** and **S2**). The binding rate of *i*-insulin toward erythrocyte ghost was evaluated. Within 2 min of the addition of Cy5-*i*-insulin to the erythrocyte ghost solution, high fluorescence intensity localized on the erythrocyte membranes was observed (*SI Appendix*, Fig. S12*A*). A concurrent rapid decrease in the fluorescence intensity of the supernatant was also observed (*SI Appendix*, Fig. S13). Next, the in vitro release kinetics of *i*-insulin was investigated by diluting the Cy5-*i*-insulin–treated erythrocyte ghost solution and observing the fluorescent signal. A sharp decrease in fluorescence intensity was noted for all Cy5-*i*-insulin–treated erythrocyte ghosts within 2 min after a twofold, fourfold, and 10-fold dilution (*SI Appendix*, Fig. S12*B*).

Cy5-*i*-insulin–treated erythrocyte ghosts were further treated with glucose solutions at varying glucose concentrations of 0, 400, 800, and 1,600 mg/dL. The fluorescence intensity gradually decreased with increased glucose concentrations, consistent with the proposed dissociation of *i*-insulin–Glut complexes (Fig. 2 *C* and *D*). The glucose-responsive dissociation of *i*-insulin–Glut complex was further tested at physiological-relevant concentrations (1 and 5 nM) of *i*-insulin (35). The concentration of *i*-insulin increased in the supernatant as the glucose concentration was increased (Fig. 2 *E* and *F*). A 100% increase in the concentration of supernatant insulin was observed as the glucose concentration increased from 0 mg/dL to 400 mg/dL for both the 1- and 5-nM concentrations.

Next, the ability of *i*-insulin to regulate blood glucose levels was evaluated in the type 1 diabetic mice induced by streptozotocin (STZ). With s.c. injection, the *i*-insulin–treated mice sustained normoglycemia below 200 mg/dL for more than 10 h (Fig. 3*A*), whereas mice treated with native insulin showed less than 4 h of normoglycemia (Fig. 3*A*). Prolonged s.c. retention of *i*-insulin at the injection site compared with native insulin was observed (*SI*

Fig. 2. The in vitro study of *i*-insulin interaction with erythrocyte ghosts. Erythrocyte ghosts were treated with sulfo-Cy5–labeled (*A*) *i*-insulin or (*B*) insulin and subsequently observed using confocal microscopy. The concentration of *i*-insulin or insulin was set as 1 μM. (Scale bar, 50 μm.) (*Insets*) The representative enlarged images. (Scale bar, 5 μm.) The fluorescence intensity on plasma membranes was analyzed using software ImageJ. (*C*) The *i*-insulin displacement by glucose. The glucose was set as 0, 400, 800, and 1,600 mg/dL. (Scale bar, 50 μm.) (*D*) The fluorescence intensity on plasma membranes was analyzed using software ImageJ. Data are presented as mean + SD ($n = 10$). (*E* and *F*) The glucose-triggered *i*-insulin release from erythrocyte ghosts. The glucose concentration was set as 0, 100, 200, 300, and 400 mg/dL, while the *i*-insulin was set as (*E*) 1 nM and (*F*) 5 nM. Human recombinant insulin ELISA kit was used to measure the *i*-insulin level in the supernatant. The average *i*-insulin level in the supernatant at 0 mg/dL of glucose was set as 100%. The data are presented as mean + SD ($n = 3$).

Appendix, Fig. S14). Of note is that mice treated with *i*-insulin showed negligible hypoglycemia (Fig. 3*A*). When a second injection of *i*-insulin or native insulin was administered 3 h posttreatment when normoglycemia was achieved, *i*-insulin–treated mice showed a significantly extended normoglycemia period with negligible hypoglycemia, while native insulin-treated mice showed marked

Fig. 3. The in vivo characterization of *i*-insulin. (*A*) The blood glucose regulation effect of s.c.-injected *i*-insulin toward STZ-induced type 1 diabetic mouse. The dose was set as 6 mg/kg. Native insulin (1.5 mg/kg) was used as a positive control. PBS was used as a negative control. Data are presented as mean ± SD ($n = 5$). The black arrow indicates the injection of *i*-insulin or insulin. (*B*) The blood glucose level change of mice treated with two sequential injections. A second injection was given at 3 h post first treatment. The doses were set to 6 and 1.5 mg/kg for *i*-insulin and insulin, respectively. Data are presented as mean ± SD ($n = 5$). The black arrows indicate the time of injection. (*C*) Hypoglycemia induction on healthy C57BL/6J mice. The doses of *i*-insulin and insulin were set as 3 and 0.75 mg/kg, respectively. The *i*-insulin and insulin were s.c. injected. Data are presented as mean ± SD ($n = 5$). The black arrow indicates the starting time of treatment. (*D* and *E*) IPGTT. The therapeutic dose was set as 6 and 1.5 mg/kg for *i*-insulin and insulin, respectively. Glucose was given at 3 h posttreatment at a dose of 1.5 g/kg. Healthy mice were used as the control. Data are presented as mean ± SD ($n = 5$). The black arrow indicates the glucose injection. The blood glucose response to IPGTT in terms of blood glucose AUC was analyzed using OriginPro 2017. The *P* values were calculated using one-way ANOVA with a Tukey post hoc test. Statistical significance *P* value was calculated to be smaller than 0.0001. ***$P < 0.001$. (*F*) IPGTT-triggered *i*-insulin release. Glucose (1.5 g/kg) was given at 3 h posttreatment. Blood plasma was collected and measured using a human insulin ELISA. The blood insulin level just before injection was set as 100%. Data were presented as mean ± SD ($n = 4$).

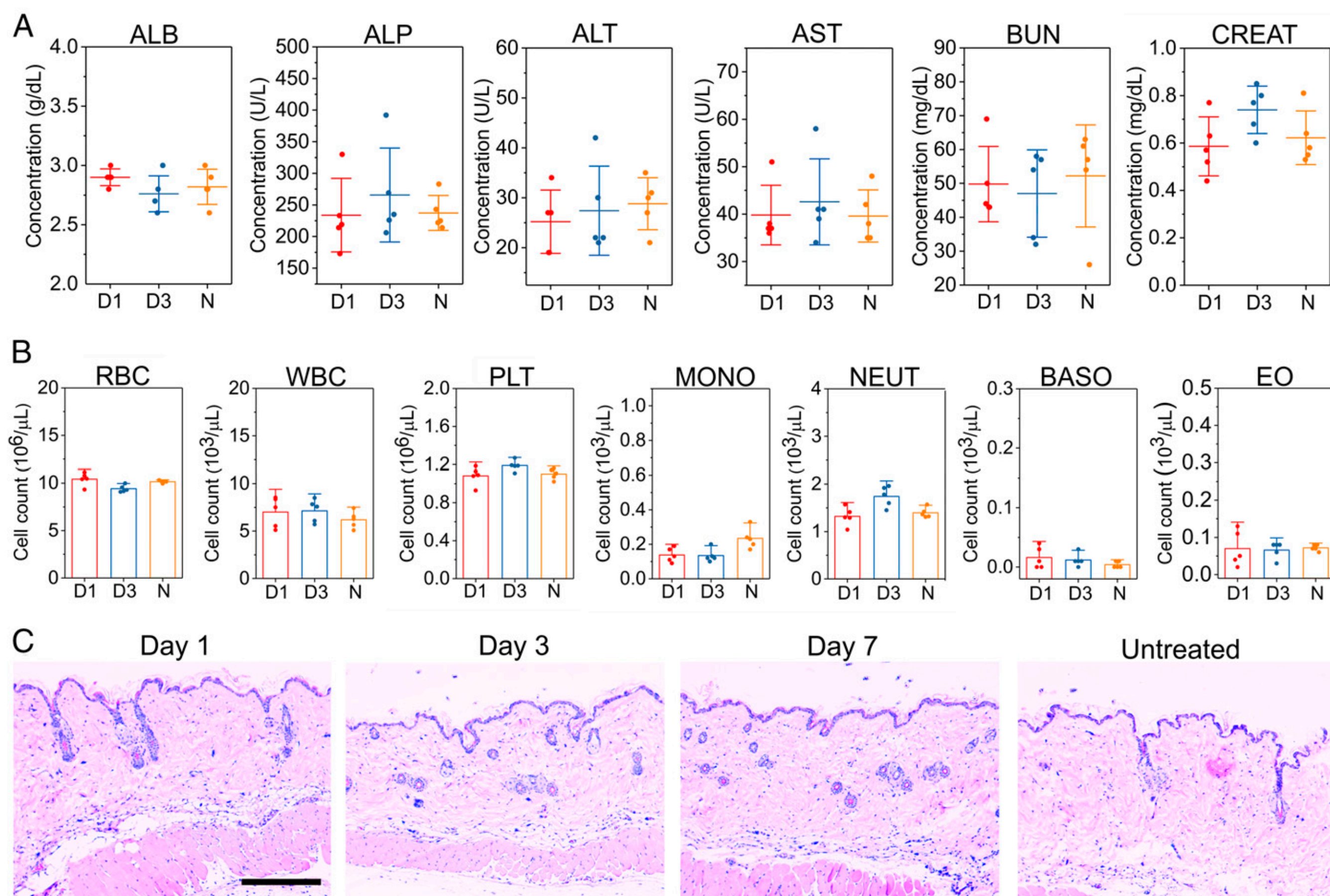

Fig. 4. Toxicity and biocompatibility evaluation of *i*-insulin in diabetic mice. (*A*) Serum ALB, ALP, ALT, AST, BUN, and CREAT concentration on day 1 or 3 posttreatment of *i*-insulin. Data are presented as mean ± SD ($n = 5$). (*B*) Red blood cell (RBC), white blood cell (WBC), platelet (PLT), monocyte (MONO), neutrophil (NEUT), basophil (BASO), and eosinophil (EO) were counted on day 1 or 3 posttreatment of *i*-insulin. D1, day 1 posttreatment; D3, day 3 posttreatment; N, no-treatment group. Data are presented as mean + SD ($n = 5$). (*C*) H&E staining of the skin, where *i*-insulin was s.c. administered, from the diabetic mice. (Scale bar, 300 μm.)

hypoglycemia (Fig. 3*B*). This hypoglycemia-mitigating effect of *i*-insulin was further evaluated on healthy mice. Following s.c. injection, native insulin induced severe hypoglycemia represented by blood glucose levels of ∼60 mg/dL. In contrast, *i*-insulin−treated mice did not show glucose levels below 100 mg/dL (Fig. 3*C*).

An i.p. glucose tolerance test (IPGTT) was also performed at 3 h posttreatment. A spike in blood glucose levels was observed for all groups; however, only *i*-insulin−treated mice and healthy mice showed blood glucose levels back to normal range within 2 h (Fig. 3*D*). The enhanced ability of *i*-insulin in regulating blood glucose levels compared with native insulin was confirmed by the area under curve (AUC) analyses (Fig. 3*E*). Moreover, a peak of plasma insulin associated with IPGTT was observed without delay in the *i*-insulin−treated mice (Fig. 3*F*).

The toxicity of *i*-insulin to the liver and kidney was further evaluated via serum albumin (ALB), alkaline phosphatase (ALP), alanine aminotransferase (ALT), aspartate transaminase (AST), blood urea nitrogen (BUN), and creatinine (CREAT) levels, on days 1 and 3 after the s.c. injection of *i*-insulin (Fig. 4*A*). No significant differences across any biochemical measures were observed. In addition, there were no obvious changes in blood cell counts (Fig. 4*B*). Meanwhile, negligible neutrophil infiltration was observed at treated skin sites, as shown in the hematoxylin and eosin (H&E) stain results (Fig. 4*C*). Moreover, the total levels of IgM and IgG associated with both healthy mice and diabetic mice were insignificantly changed during the 2-wk treatment (*SI Appendix*, Fig. S15) (36, 37). Systemic evaluation of the specific immune responses against *i*-insulin upon variation of treatment doses, frequencies, and routes are required for further translation (37, 38).

Discussion

Bioresponsive insulin-mediated treatment has the potential to revolutionize the current diabetes treatment. An insulin molecule with the properties of glucose responsiveness and hypoglycemia mitigation would offer a novel approach to regulate blood glucose levels with low risk for hypoglycemia. In this study, we engineered such a molecule via conjugation of insulin to the Glut competitive inhibitor Glut-i2 to allow *i*-insulin for reversible and glucose-responsive binding to endogenous Glut. In vitro, the *i*-insulin was able to rapidly bind to Glut on erythrocyte ghosts at low blood glucose concentrations, while releasing free and glucose-accessible Glut in response to hyperglycemia. Upon a glucose challenge, *i*-insulin was liberated from the *i*-insulin−Glut complex for subsequent binding to IR and rapid blood glucose clearance.

Upon s.c. injection in type 1 diabetic mice, *i*-insulin showed a significantly more durable normoglycemia effect with negligible hypoglycemia, even after a second injection. This result was further confirmed with studies showing that *i*-insulin only slightly lowered blood glucose of healthy mice, while native insulin induced severe hypoglycemia. Upon a glucose challenge, a portion of *i*-insulin was released from *i*-insulin−Glut complex directly to the interstitial fluid and plasma. Remarkably, the direct release

of *i*-insulin to the interstitial environment may help *i*-insulin rapidly reach IRs on target cells. In addition, the release of *i*-insulin from the *i*-insulin–Glut complex generates glucose-accessible free Glut to enhance the excess glucose clearance from blood.

This glucose transporter inhibitor-mediated insulin can be further optimized, regarding response kinetics, effective duration, and Glut specificity, through varying the component(s) of glucose transporter inhibitor, insulin, and spacer. Moreover, this glucose-responsive insulin can be further integrated with painless transdermal microneedle array patch to generate a new version of "smart insulin patch" (*SI Appendix*, Fig. S16) (39, 40) or oral delivery systems to form "smart insulin pills" (41).

Materials and Methods

Experimental procedures for insulin analog synthesis and in vitro glucose-triggered insulin release, procedures for animal experiment, and additional control experiments are provided in *SI Appendix*. The animal study protocol was approved by the Institutional Animal Care and Use Committee at North Carolina State University and the University of California, Los Angeles.

ACKNOWLEDGMENTS. This work was supported by National Institutes of Health Grants R01 DK112939 01A1 and UL1TR002489; Juvenile Diabetes Research Foundation Grant 2-SRA-2016-269-A-N; and grants from the start-up packages of University of California, Los Angeles. J.P.W. thanks the University of California, San Diego/University of California, Los Angeles National Institute of Diabetes and Digestive and Kidney Diseases Diabetes Research Center Grant P30 DK063491 for support.

1. Reusch JE, Manson JE (2017) Management of type 2 diabetes in 2017: Getting to goal. *JAMA* 317:1015–1016.
2. Yu J, Zhang Y, Bomba H, Gu Z (2016) Stimuli-responsive delivery of therapeutics for diabetes treatment. *Bioeng Transl Med* 1:323–337.
3. VandenBerg MA, Webber MJ (January 3, 2019) Biologically inspired and chemically derived methods for glucose-responsive insulin therapy. *Adv Healthc Mater*10.1002/adhm.201801466.
4. Wagner AM, Gran MP, Peppas NA (2018) Designing the new generation of intelligent biocompatible carriers for protein and peptide delivery. *Acta Pharm Sin B* 8:147–164.
5. Cryer P (2016) *Hypoglycemia in Diabetes: Pathophysiology, Prevalence, and Prevention* (American Diabetes Assoc, Arlington, VA).
6. Bakh NA, et al. (2017) Glucose-responsive insulin by molecular and physical design. *Nat Chem* 9:937–943.
7. Lu Y, Aimetti AA, Langer R, Gu Z (2017) Bioresponsive materials. *Nat Rev Mater* 2: 16075.
8. Shiino D, et al. (1995) Amine containing phenylboronic acid gel for glucose-responsive insulin release under physiological pH. *J Control Release* 37:269–276.
9. Matsumoto A, et al. (2012) A synthetic approach toward a self-regulated insulin delivery system. *Angew Chem Int Ed Engl* 51:2124–2128.
10. Chou DH, et al. (2015) Glucose-responsive insulin activity by covalent modification with aliphatic phenylboronic acid conjugates. *Proc Natl Acad Sci USA* 112:2401–2406.
11. Dong Y, et al. (2016) Injectable and glucose-responsive hydrogels based on boronic acid-glucose complexation. *Langmuir* 32:8743–8747.
12. Veiseh O, Tang BC, Whitehead KA, Anderson DG, Langer R (2015) Managing diabetes with nanomedicine: Challenges and opportunities. *Nat Rev Drug Discov* 14:45–57.
13. Chen S, et al. (2018) Microneedle-array patch fabricated with enzyme-free polymeric components capable of on-demand insulin delivery. *Adv Funct Mater* 29:1807369.
14. Matsumoto A, et al. (2017) Synthetic "smart gel" provides glucose-responsive insulin delivery in diabetic mice. *Sci Adv* 3:eaaq0723.
15. Matsumoto A, et al. (2010) A totally synthetic glucose responsive gel operating in physiological aqueous conditions. *Chem Commun (Camb)* 46:2203–2205.
16. Matsumoto A, Yoshida R, Kataoka K (2004) Glucose-responsive polymer gel bearing phenylborate derivative as a glucose-sensing moiety operating at the physiological pH. *Biomacromolecules* 5:1038–1045.
17. Wang C, et al. (2017) Red blood cells for glucose-responsive insulin delivery. *Adv Mater* 29:1606617.
18. Brownlee M, Cerami A (1979) A glucose-controlled insulin-delivery system: Semi-synthetic insulin bound to lectin. *Science* 206:1190–1191.
19. Kaarsholm NC, et al. (2018) Engineering glucose responsiveness into insulin. *Diabetes* 67:299–308.
20. Yang R, et al. (2018) A glucose-responsive insulin therapy protects animals against hypoglycemia. *JCI Insight* 3:e97476.
21. Fischel-Ghodsian F, Brown L, Mathiowitz E, Brandenburg D, Langer R (1988) Enzymatically controlled drug delivery. *Proc Natl Acad Sci USA* 85:2403–2406.
22. Wang J, et al. (2018) Core-shell microneedle gel for self-regulated insulin delivery. *ACS Nano* 12:2466–2473.
23. Podual K, Doyle FJ III, Peppas NA (2000) Glucose-sensitivity of glucose oxidase-containing cationic copolymer hydrogels having poly(ethylene glycol) grafts. *J Control Release* 67:9–17.
24. Podual K, Doyle FJ III, Peppas NA (2000) Preparation and dynamic response of cationic copolymer hydrogels containing glucose oxidase. *Polymer (Guildf)* 41:3975–3983.
25. Podual K, Doyle FJ III, Peppas NA (2000) Dynamic behavior of glucose oxidase-containing microparticles of poly(ethylene glycol)-grafted cationic hydrogels in an environment of changing pH. *Biomaterials* 21:1439–1450.
26. Gu Z, et al. (2013) Injectable nano-network for glucose-mediated insulin delivery. *ACS Nano* 7:4194–4201.
27. Yu J, Zhang Y, Yan J, Kahkoska AR, Gu Z (2018) Advances in bioresponsive closed-loop drug delivery systems. *Int J Pharm* 544:350–357.
28. Gould GW, Holman GD (1993) The glucose transporter family: Structure, function and tissue-specific expression. *Biochem J* 295:329–341.
29. Granchi C, Fortunato S, Minutolo F (2016) Anticancer agents interacting with membrane glucose transporters. *MedChemComm* 7:1716–1729.
30. Siebeneicher H, et al. (2016) Identification of novel GLUT inhibitors. *Bioorg Med Chem Lett* 26:1732–1737.
31. Chan DA, et al. (2011) Targeting GLUT1 and the Warburg effect in renal cell carcinoma by chemical synthetic lethality. *Sci Transl Med* 3:94ra70.
32. Kapoor K, et al. (2016) Mechanism of inhibition of human glucose transporter GLUT1 is conserved between cytochalasin B and phenylalanine amides. *Proc Natl Acad Sci USA* 113:4711–4716.
33. Jung CY, Rampal AL (1977) Cytochalasin B binding sites and glucose transport carrier in human erythrocyte ghosts. *J Biol Chem* 252:5456–5463.
34. Kasahara M, Hinkle PC (1977) Reconstitution and purification of the D-glucose transporter from human erythrocytes. *J Biol Chem* 252:7384–7390.
35. Olefsky J, Farquhar JW, Reaven G (1973) Relationship between fasting plasma insulin level and resistance to insulin-mediated glucose uptake in normal and diabetic subjects. *Diabetes* 22:507–513.
36. Yang W, et al. (2014) Poly(carboxybetaine) nanomaterials enable long circulation and prevent polymer-specific antibody production. *Nano Today* 9:10–16.
37. Torosantucci R, et al. (2014) Development of a transgenic mouse model to study the immunogenicity of recombinant human insulin. *J Pharm Sci* 103:1367–1374.
38. Ottesen JL, et al. (1994) The potential immunogenicity of human insulin and insulin analogues evaluated in a transgenic mouse model. *Diabetologia* 37:1178–1185.
39. Yu J, et al. (2015) Microneedle-array patches loaded with hypoxia-sensitive vesicles provide fast glucose-responsive insulin delivery. *Proc Natl Acad Sci USAProc Natl Acad Sci USA* 112:8260–8265.
40. Veiseh O, Langer R, et al. (2015) Diabetes: A smart insulin patch. *Nature* 524:39–40.
41. Yu J, et al. (December 18, 2018) Glucose-responsive oral insulin delivery for postprandial glycemic regulation. *Nano Res*, 10.1007/s12274-018-2264-9.